Measurement of the asymmetry in angular distributions of leptons produced in dilepton $t\bar{t}$ final states in $p\bar{p}$ collisions at $\sqrt{s} = 1.96$ TeV

V. M. Abazov,[31] B. Abbott,[66] B. S. Acharya,[25] M. Adams,[45] T. Adams,[43] J. P. Agnew,[40] G. D. Alexeev,[31] G. Alkhazov,[35] A. Alton,[55,*] A. Askew,[43] S. Atkins,[53] K. Augsten,[7] C. Avila,[5] F. Badaud,[10] L. Bagby,[44] B. Baldin,[44] D. V. Bandurin,[43] S. Banerjee,[25] E. Barberis,[54] P. Baringer,[52] J. F. Bartlett,[44] U. Bassler,[15] V. Bazterra,[45] A. Bean,[52] M. Begalli,[2] L. Bellantoni,[44] S. B. Beri,[23] G. Bernardi,[14] R. Bernhard,[19] I. Bertram,[38] M. Besançon,[15] R. Beuselinck,[39] P. C. Bhat,[44] S. Bhatia,[57] V. Bhatnagar,[23] G. Blazey,[46] S. Blessing,[43] K. Bloom,[58] A. Boehnlein,[44] D. Boline,[63] E. E. Boos,[33] G. Borissov,[38] A. Brandt,[69] O. Brandt,[20] R. Brock,[56] A. Bross,[44] D. Brown,[14] X. B. Bu,[44] M. Buehler,[44] V. Buescher,[21] V. Bunichev,[33] S. Burdin,[38,†] C. P. Buszello,[37] E. Camacho-Pérez,[28] B. C. K. Casey,[44] H. Castilla-Valdez,[28] S. Caughron,[56] S. Chakrabarti,[63] K. M. Chan,[50] A. Chandra,[71] A. Chapelain,[15] E. Chapon,[15] G. Chen,[52] S. W. Cho,[27] S. Choi,[27] B. Choudhary,[24] S. Cihangir,[44] D. Claes,[58] J. Clutter,[52] M. Cooke,[44] W. E. Cooper,[44] M. Corcoran,[71] F. Couderc,[15] M.-C. Cousinou,[12] D. Cutts,[68] A. Das,[41] G. Davies,[39] S. J. de Jong,[29,30] E. De La Cruz-Burelo,[28] F. Déliot,[15] R. Demina,[62] D. Denisov,[44] S. P. Denisov,[34] S. Desai,[44] C. Deterre,[20,‡] K. DeVaughan,[58] H. T. Diehl,[44] M. Diesburg,[44] P. F. Ding,[40] A. Dominguez,[58] A. Dubey,[24] L. V. Dudko,[33] A. Duperrin,[12] S. Dutt,[23] M. Eads,[46] D. Edmunds,[56] J. Ellison,[42] V. D. Elvira,[44] Y. Enari,[14] H. Evans,[48] V. N. Evdokimov,[34] A. Falkowski,[15,‖] L. Feng,[46] T. Ferbel,[62] F. Fiedler,[21] F. Filthaut,[29,30] W. Fisher,[56] H. E. Fisk,[44] M. Fortner,[46] H. Fox,[38] S. Fuess,[44] P. H. Garbincius,[44] A. Garcia-Bellido,[62] J. A. García-González,[28] V. Gavrilov,[32] W. Geng,[12,56] C. E. Gerber,[45] Y. Gershtein,[59] G. Ginther,[44,62] G. Golovanov,[31] P. D. Grannis,[63] S. Greder,[16] H. Greenlee,[44] G. Grenier,[17] Ph. Gris,[10] J.-F. Grivaz,[13] A. Grohsjean,[15,‡] S. Grünendahl,[44] M. W. Grünewald,[26] T. Guillemin,[13] G. Gutierrez,[44] P. Gutierrez,[66] J. Haley,[66] L. Han,[4] K. Harder,[40] A. Harel,[62] J. M. Hauptman,[51] J. Hays,[39] T. Head,[40] T. Hebbeker,[18] D. Hedin,[46] H. Hegab,[67] A. P. Heinson,[42] U. Heintz,[68] C. Hensel,[20] I. Heredia-De La Cruz,[28,§] K. Herner,[44] G. Hesketh,[40,¶] M. D. Hildreth,[50] R. Hirosky,[72] T. Hoang,[43] J. D. Hobbs,[63] B. Hoeneisen,[9] J. Hogan,[71] M. Hohlfeld,[21] J. L. Holzbauer,[57] I. Howley,[69] Z. Hubacek,[7,15] V. Hynek,[7] I. Iashvili,[61] Y. Ilchenko,[70] R. Illingworth,[44] A. S. Ito,[44] S. Jabeen,[68] M. Jaffré,[13] A. Jayasinghe,[66] M. S. Jeong,[27] R. Jesik,[39] P. Jiang,[4] K. Johns,[41] E. Johnson,[56] M. Johnson,[44] A. Jonckheere,[44] P. Jonsson,[39] J. Joshi,[42] A. W. Jung,[44] A. Juste,[36] E. Kajfasz,[12] D. Karmanov,[33] I. Katsanos,[58] R. Kehoe,[70] S. Kermiche,[12] N. Khalatyan,[44] A. Khanov,[67] A. Kharchilava,[61] Y. N. Kharzheev,[31] I. Kiselevich,[32] J. M. Kohli,[23] A. V. Kozelov,[34] J. Kraus,[57] A. Kumar,[61] A. Kupco,[8] T. Kurča,[17] V. A. Kuzmin,[33] S. Lammers,[48] P. Lebrun,[17] H. S. Lee,[27] S. W. Lee,[51] W. M. Lee,[44] X. Lei,[41] J. Lellouch,[14] D. Li,[14] H. Li,[72] L. Li,[42] Q. Z. Li,[44] J. K. Lim,[27] D. Lincoln,[44] J. Linnemann,[56] V. V. Lipaev,[34] R. Lipton,[44] H. Liu,[70] Y. Liu,[4] A. Lobodenko,[35] M. Lokajicek,[8] R. Lopes de Sa,[63] R. Luna-Garcia,[28,**] A. L. Lyon,[44] A. K. A. Maciel,[1] R. Madar,[19] R. Magaña-Villalba,[28] S. Malik,[58] V. L. Malyshev,[31] J. Mansour,[20] J. Martínez-Ortega,[28] R. McCarthy,[63] C. L. McGivern,[40] M. M. Meijer,[29,30] A. Melnitchouk,[44] D. Menezes,[46] P. G. Mercadante,[3] M. Merkin,[33] A. Meyer,[18] J. Meyer,[20,‡‡] F. Miconi,[16] N. K. Mondal,[25] M. Mulhearn,[72] E. Nagy,[12] M. Narain,[68] R. Nayyar,[41] H. A. Neal,[55] J. P. Negret,[5] P. Neustroev,[35] H. T. Nguyen,[72] T. Nunnemann,[22] J. Orduna,[71] N. Osman,[12] J. Osta,[50] A. Pal,[69] N. Parashar,[49] V. Parihar,[68] S. K. Park,[27] R. Partridge,[68,‖] N. Parua,[48] A. Patwa,[64,§§] B. Penning,[44] M. Perfilov,[33] Y. Peters,[20] K. Petridis,[40] G. Petrillo,[62] P. Pétroff,[13] M.-A. Pleier,[64] V. M. Podstavkov,[44] A. V. Popov,[34] M. Prewitt,[71] D. Price,[40] N. Prokopenko,[34] J. Qian,[55] A. Quadt,[20] B. Quinn,[57] P. N. Ratoff,[38] I. Razumov,[34] I. Ripp-Baudot,[16] F. Rizatdinova,[67] M. Rominsky,[44] A. Ross,[38] C. Royon,[15] P. Rubinov,[44] R. Ruchti,[50] G. Sajot,[11] A. Sánchez-Hernández,[28] M. P. Sanders,[22] A. S. Santos,[1,††] G. Savage,[44] L. Sawyer,[53] T. Scanlon,[39] R. D. Schamberger,[63] Y. Scheglov,[35] H. Schellman,[47] C. Schwanenberger,[40] R. Schwienhorst,[56] J. Sekaric,[52] H. Severini,[66] E. Shabalina,[20] V. Shary,[15] S. Shaw,[56] A. A. Shchukin,[34] V. Simak,[7] P. Skubic,[66] P. Slattery,[62] D. Smirnov,[50] G. R. Snow,[58] J. Snow,[65] S. Snyder,[64] S. Söldner-Rembold,[40] L. Sonnenschein,[18] K. Soustruznik,[6] J. Stark,[11] D. A. Stoyanova,[34] M. Strauss,[66] L. Suter,[40] P. Svoisky,[66] M. Titov,[15] V. V. Tokmenin,[31] Y.-T. Tsai,[62] D. Tsybychev,[63] B. Tuchming,[15] C. Tully,[60] L. Uvarov,[35] S. Uvarov,[35] S. Uzunyan,[46] R. Van Kooten,[48] W. M. van Leeuwen,[29] N. Varelas,[45] E. W. Varnes,[41] I. A. Vasilyev,[34] A. Y. Verkheev,[31] L. S. Vertogradov,[31] M. Verzocchi,[44] M. Vesterinen,[40] D. Vilanova,[15] P. Vokac,[7] H. D. Wahl,[43] M. H. L. S. Wang,[44] J. Warchol,[50] G. Watts,[73] M. Wayne,[50] J. Weichert,[21] L. Welty-Rieger,[47] M. R. J. Williams,[48] G. W. Wilson,[52] M. Wobisch,[53] D. R. Wood,[54] T. R. Wyatt,[40] Y. Xie,[44] R. Yamada,[44] S. Yang,[4] T. Yasuda,[44] Y. A. Yatsunenko,[31] W. Ye,[63] Z. Ye,[44] H. Yin,[44] K. Yip,[64] S. W. Youn,[44] J. M. Yu,[55] J. Zennamo,[61] T. G. Zhao,[40] B. Zhou,[55] J. Zhu,[55] M. Zielinski,[62] D. Zieminska,[48] and L. Zivkovic[14]

(D0 Collaboration)

[1]*LAFEX, Centro Brasileiro de Pesquisas Físicas, Rio de Janeiro, Brazil*
[2]*Universidade do Estado do Rio de Janeiro, Rio de Janeiro, Brazil*
[3]*Universidade Federal do ABC, Santo André, Brazil*
[4]*University of Science and Technology of China, Hefei, People's Republic of China*
[5]*Universidad de los Andes, Bogotá, Colombia*
[6]*Charles University, Faculty of Mathematics and Physics, Center for Particle Physics, Prague, Czech Republic*
[7]*Czech Technical University in Prague, Prague, Czech Republic*
[8]*Institute of Physics, Academy of Sciences of the Czech Republic, Prague, Czech Republic*
[9]*Universidad San Francisco de Quito, Quito, Ecuador*
[10]*LPC, Université Blaise Pascal, CNRS/IN2P3, Clermont, France*
[11]*LPSC, Université Joseph Fourier Grenoble 1, CNRS/IN2P3, Institut National Polytechnique de Grenoble, Grenoble, France*
[12]*CPPM, Aix-Marseille Université, CNRS/IN2P3, Marseille, France*
[13]*LAL, Université Paris-Sud, CNRS/IN2P3, Orsay, France*
[14]*LPNHE, Universités Paris VI and VII, CNRS/IN2P3, Paris, France*
[15]*CEA, Irfu, SPP, Saclay, France*
[16]*IPHC, Université de Strasbourg, CNRS/IN2P3, Strasbourg, France*
[17]*IPNL, Université Lyon 1, CNRS/IN2P3, Villeurbanne, France and Université de Lyon, Lyon, France*
[18]*III. Physikalisches Institut A, RWTH Aachen University, Aachen, Germany*
[19]*Physikalisches Institut, Universität Freiburg, Freiburg, Germany*
[20]*II. Physikalisches Institut, Georg-August-Universität Göttingen, Göttingen, Germany*
[21]*Institut für Physik, Universität Mainz, Mainz, Germany*
[22]*Ludwig-Maximilians-Universität München, München, Germany*
[23]*Panjab University, Chandigarh, India*
[24]*Delhi University, Delhi, India*
[25]*Tata Institute of Fundamental Research, Mumbai, India*
[26]*University College Dublin, Dublin, Ireland*
[27]*Korea Detector Laboratory, Korea University, Seoul, Korea*
[28]*CINVESTAV, Mexico City, Mexico*
[29]*Nikhef, Science Park, Amsterdam, The Netherlands*
[30]*Radboud University Nijmegen, Nijmegen, The Netherlands*
[31]*Joint Institute for Nuclear Research, Dubna, Russia*
[32]*Institute for Theoretical and Experimental Physics, Moscow, Russia*
[33]*Moscow State University, Moscow, Russia*
[34]*Institute for High Energy Physics, Protvino, Russia*
[35]*Petersburg Nuclear Physics Institute, St. Petersburg, Russia*
[36]*Institució Catalana de Recerca i Estudis Avançats (ICREA) and Institut de Física d'Altes Energies (IFAE), Barcelona, Spain*
[37]*Uppsala University, Uppsala, Sweden*
[38]*Lancaster University, Lancaster LA1 4YB, United Kingdom*
[39]*Imperial College London, London SW7 2AZ, United Kingdom*
[40]*The University of Manchester, Manchester M13 9PL, United Kingdom*
[41]*University of Arizona, Tucson, Arizona 85721, USA*
[42]*University of California Riverside, Riverside, California 92521, USA*
[43]*Florida State University, Tallahassee, Florida 32306, USA*
[44]*Fermi National Accelerator Laboratory, Batavia, Illinois 60510, USA*
[45]*University of Illinois at Chicago, Chicago, Illinois 60607, USA*
[46]*Northern Illinois University, DeKalb, Illinois 60115, USA*
[47]*Northwestern University, Evanston, Illinois 60208, USA*
[48]*Indiana University, Bloomington, Indiana 47405, USA*
[49]*Purdue University Calumet, Hammond, Indiana 46323, USA*
[50]*University of Notre Dame, Notre Dame, Indiana 46556, USA*
[51]*Iowa State University, Ames, Iowa 50011, USA*
[52]*University of Kansas, Lawrence, Kansas 66045, USA*
[53]*Louisiana Tech University, Ruston, Louisiana 71272, USA*
[54]*Northeastern University, Boston, Massachusetts 02115, USA*
[55]*University of Michigan, Ann Arbor, Michigan 48109, USA*
[56]*Michigan State University, East Lansing, Michigan 48824, USA*
[57]*University of Mississippi, University, Mississippi 38677, USA*
[58]*University of Nebraska, Lincoln, Nebraska 68588, USA*
[59]*Rutgers University, Piscataway, New Jersey 08855, USA*
[60]*Princeton University, Princeton, New Jersey 08544, USA*
[61]*State University of New York, Buffalo, New York 14260, USA*

[62]*University of Rochester, Rochester, New York 14627, USA*
[63]*State University of New York, Stony Brook, New York 11794, USA*
[64]*Brookhaven National Laboratory, Upton, New York 11973, USA*
[65]*Langston University, Langston, Oklahoma 73050, USA*
[66]*University of Oklahoma, Norman, Oklahoma 73019, USA*
[67]*Oklahoma State University, Stillwater, Oklahoma 74078, USA*
[68]*Brown University, Providence, Rhode Island 02912, USA*
[69]*University of Texas, Arlington, Texas 76019, USA*
[70]*Southern Methodist University, Dallas, Texas 75275, USA*
[71]*Rice University, Houston, Texas 77005, USA*
[72]*University of Virginia, Charlottesville, Virginia 22904, USA*
[73]*University of Washington, Seattle, Washington 98195, USA*

We present measurements of asymmetries in angular distributions of leptons produced in $t\bar{t}$ events in proton-antiproton collisions at the Fermilab Tevatron Collider. We consider final states where the $W^{\pm}$ bosons from top quark and antiquark decays both decay into $\ell\nu$ ($\ell = e, \mu$) resulting in oppositely charged dilepton final states with accompanying jets. Using 9.7 fb^{-1} of integrated luminosity collected with the D0 detector, we find the asymmetries in lepton pseudorapidity compatible with predictions based on the standard model.

The top quark, first observed by the CDF and D0 Collaborations in 1995 [1,2], is the heaviest of all elementary particles. Due to the large top quark mass, the measurement of the production and decay properties of top quark pairs in proton-antiproton ($p\bar{p}$) collisions provides an important test of the standard model (SM) of particle physics that may unveil the presence of new phenomena beyond the SM (BSM).

Perturbative quantum chromodynamics (pQCD) at leading order (LO) predicts that top quark-antiquark ($t\bar{t}$) production in quark-antiquark ($q\bar{q}$) annihilation in the center of mass frame is forward-backward (FB) symmetric in the angular distributions of the t and $\bar{t}$ quarks. However, a positive FB asymmetry appears from next-to-leading order (NLO) contributions [3–6], such that the top (antitop) quark is preferentially emitted in the direction of the

incoming quark (antiquark). Processes beyond the SM can modify the $t\bar{t}$ production asymmetry, for example through contributions from axigluons or diquarks [7–19], Z'/W' bosons [20–28], supersymmetry [29–31], or new scalar particles [32,33]. The CDF and D0 Collaborations have performed measurements of the $t\bar{t}$ FB asymmetry in $t\bar{t}$ decaying to $\ell +$ jets final states containing jets, an imbalance in transverse energy ($\not{E}_T$), and just one lepton ($\ell = e$ or μ) from W decay where the W is coming from t or $\bar{t}$, based on data corresponding to integrated luminosities of 9.4 fb^{-1} [34] and 5.4 fb^{-1} [35], respectively. The FB asymmetries reported by the CDF and D0 Collaborations both differ by more than two standard deviations (SDs) from the NLO pQCD predictions [34,35].

Rather than measuring the FB asymmetry of the top quarks themselves, an asymmetry in $t\bar{t}$ events can also be measured from the pseudorapidity [36] of the single charged lepton in the $\ell +$ jets final state. In such a measurement, based on an integrated luminosity of 9.4 fb^{-1} and 5.4 fb^{-1}, CDF and D0 found deviations from NLO pQCD predictions of about 3 SDs [35] and of 1.7 SDs [37], respectively. The D0 Collaboration also reported a similar measurement in dilepton final states [38], where the W bosons from t and $\bar{t}$ decays both decay into $\ell\nu$ ($\ell = e$ or μ), in data corresponding to an integrated luminosity of 5.4 fb^{-1}. The asymmetry results reported in Ref. [38], combined with the measurement in the $\ell +$ jets final state, reduce the disagreement with the NLO pQCD predictions to 2.2 SDs [38].

The results of the ATLAS and CMS Collaborations based on the difference of top and antitop quark production angles in the $\ell +$ jets final states show good agreement with NLO pQCD expectations in proton-proton collisions at $\sqrt{s} = 7$ TeV [39,40]. However, at the LHC, measured

————
*Visitor from Augustana College, Sioux Falls, South Dakota, USA.
†Visitor from The University of Liverpool, Liverpool, United Kingdom.
‡Visitor from DESY, Hamburg, Germany.
§Visitor from Universidad Michoacana de San Nicolas de Hidalgo, Morelia, Mexico.
∥Visitor from SLAC, Menlo Park, California, USA.
¶Visitor from University College London, London, United Kingdom.
**Visitor from Centro de Investigacion en Computacion - IPN, Mexico City, Mexico.
††Visitor from Universidade Estadual Paulista, São Paulo, Brazil.
‡‡Visitor from Karlsruher Institut für Technologie (KIT) - Steinbuch Centre for Computing (SCC).
§§Visitor from Office of Science, U.S. Department of Energy, Washington, D.C. 20585, USA.
∥∥Visitor from Laboratoire de Physique Theorique, Orsay, France.

asymmetries in top quark angular distributions are not directly comparable with the values extracted at the Tevatron, because of the symmetry of the initial proton-proton state at the LHC. This symmetry at the LHC leads to a weaker sensitivity to the physics process responsible for the production asymmetry compared to the Tevatron.

In this article, we report a new measurement of the asymmetry in the pseudorapidity distributions of leptons produced in $t\bar{t}$ events in the dilepton channel, based on all the data collected by the D0 Collaboration in Run II of the Tevatron corresponding to an integrated luminosity of 9.7 fb^{-1} following relevant data quality selection, and we compare our results with the most recent predictions based on the standard model [41].

We use the two observables $q \times \eta$ and $\Delta\eta$, where q and η are the charge and pseudorapidity of the lepton, and $\Delta\eta = \eta_{\ell^+} - \eta_{\ell^-}$ is the difference in lepton pseudorapidities. The single-lepton asymmetry A_{FB}^{ℓ} is defined as

$$A_{\text{FB}}^{\ell} = \frac{N(q \times \eta > 0) - N(q \times \eta < 0)}{N(q \times \eta > 0) + N(q \times \eta < 0)}, \quad (1)$$

where N corresponds to the number of leptons satisfying a given set of selection criteria. In this asymmetry, the positive and negative leptons in the event each contribute independently. The dilepton asymmetry $A^{\ell\ell}$ is defined as

$$A^{\ell\ell} = \frac{N(\Delta\eta > 0) - N(\Delta\eta < 0)}{N(\Delta\eta > 0) + N(\Delta\eta < 0)}. \quad (2)$$

The A_{FB}^{ℓ} and $A^{\ell\ell}$ asymmetries are highly correlated as we discuss in Sec. VI.

I. THE D0 DETECTOR AND OBJECT IDENTIFICATION

The D0 detector [42–44] has a central tracking system consisting of a silicon microstrip tracker and a central fiber tracker, both located within a 2 T superconducting solenoidal magnet. The central tracking system is designed to optimize tracking and vertexing at detector pseudorapidities (relative to the center of the D0 detector) of $|\eta_{\text{det}}| < 3$ and $|\eta_{\text{det}}| < 2.5$, respectively. A liquid-argon sampling calorimeter has a central section (CC) covering pseudorapidities $|\eta_{\text{det}}|$ up to ≈ 1.1, and two end calorimeters (ECs) that extend coverage to $|\eta_{\text{det}}| \approx 4.2$, with all three housed in separate cryostats [45]. An outer muon system, at $|\eta_{\text{det}}| < 2$, consists of a layer of tracking detectors and scintillation trigger counters in front of 1.8 T toroids, followed by two similar layers after the toroids [46].

In the current analysis, we focus on $t\bar{t}$ dilepton final states that contain two isolated charged leptons (ee, $e\mu$, or $\mu\mu$), at least two candidate b-quark jets, and significant $\not{E}_T$ attributed to escaping neutrinos. Electrons are identified as energy clusters in the calorimeter within a cone of radius $\mathcal{R} = \sqrt{(\Delta\eta)^2 + (\Delta\phi)^2} = 0.2$ (with ϕ the azimuthal angle), that are consistent in their longitudinal and transverse

profiles with those expected of an electromagnetic shower. More than 90% of the energy of an electron candidate must be deposited in the electromagnetic part of the calorimeter. Electrons are required to be isolated by demanding that less than 20% of their energy be deposited in an annulus of $0.2 < \mathcal{R} < 0.4$ around their direction. This cluster has to be matched to a track reconstructed in the central tracking system. We consider electrons in the CC with $|\eta_{\text{det}}| < 1.1$ and in the EC with $1.5 < |\eta_{\text{det}}| < 2.5$. Transverse momentum p_T of electrons must be greater than 15 GeV. In addition, we use an electron multivariate discriminant based on tracking and calorimeter information, to reject jets misidentified as electrons. It has a 75%–80% efficiency to select real electrons, and a rejection $\approx 96\%$ for misidentified jets.

A muon is identified [47] as a segment in at least one layer of the muon system that is matched to a track reconstructed in the central tracking system. Reconstructed muons must have $p_T > 15$ GeV and satisfy two isolation criteria. First, the transverse energy deposited in the calorimeter annulus around the muon $0.1 < \mathcal{R} < 0.4$ ($E_T^{\mu,\text{iso}}$) has to be less than 15% of the transverse momentum of the muon (p_T^{μ}). Second, the sum of the transverse momenta of the tracks in a cone of radius $\mathcal{R} = 0.5$ around the muon track in the central tracking system ($p_T^{\mu,\text{iso}}$) has to be less than 15% of p_T^{μ}.

Jets are identified as energy clusters in the electromagnetic and hadronic parts of the calorimeter reconstructed using an iterative midpoint cone algorithm with radius $\mathcal{R} = 0.5$ [48] and $|\eta_{\text{det}}| < 2.5$. A jet energy scale correction is determined by calibrating the energy deposited in the jet cone using transverse momentum balance in photon + jet and dijet events. When a muon track overlaps the jet cone, the momentum of that muon is added to the jet p_T, assuming that the muon originates from the semileptonic decay of a hadron belonging to the jet. Jets in simulated events are corrected for residual differences in energy resolution and energy scale between data and simulation. These correction factors are measured by comparing data and simulation in Drell-Yan ($Z/\gamma^\star \to ee$) plus jets events.

We use a multivariate analysis (MVA) to identify jets originating from b quarks [49]. The algorithm combines into a single discriminant variable the information from the impact parameters of tracks and from variables that characterize the properties of secondary vertices within jets using a single discriminant. Jet candidates for b tagging are required to have at least two tracks with $p_T > 0.5$ GeV originating from the vertex of the $p\bar{p}$ interaction and to be matched to a jet reconstructed from the tracks.

The $\not{E}_T$ is reconstructed from the energy deposited in the calorimeter cells, and corrections to p_T for leptons and jets are propagated into the $\not{E}_T$. A significance in $\not{E}_T$ [$\mathcal{S}(\not{E}_T)$] is defined for each event through a likelihood discriminant constructed from the ratio of the $\not{E}_T$ to its uncertainty.

II. SIMULATED EVENTS

Monte Carlo (MC) events are processed through a GEANT-based [50] simulation of the D0 detector. To simulate effects from additional overlapping $p\bar{p}$ interactions, "zero bias" events are selected randomly in collider data and overlaid on the fully simulated MC events. Residual differences between data and simulation of electron and muon p_T resolution and identification are corrected by comparing $Z/\gamma^{\star} \to \ell\ell$ events in data and MC, applying tight requirements on one of the two leptons and using the other one to measure efficiencies and resolutions.

We use the NLO generator MC@NLO 3.4 [51,52], interfaced with HERWIG 6.510 [53] for parton showering and hadronization, to simulate $t\bar{t}$ events. The main sources of background in the dilepton channel correspond to $q\bar{q} \to Z/\gamma^{\star} \to \ell\ell$, diboson production (*WW, WZ, ZZ*), and instrumental background. The instrumental background arises mainly from multijet and $(W \to \ell\nu)$ + jets events in which one or two jets are misidentified as electrons or where muons or electrons originating from the semileptonic decay of a heavy-flavor hadron appear isolated. This background is evaluated using data, as described in Sec. III. $Z/\gamma^{\star}$ events are generated with the tree-level LO matrix element generator ALPGEN v2.11 [54] interfaced with PYTHIA 6.409 [55] (D0 modified tune A [56]) for parton showering and hadronization. Diboson events are generated with PYTHIA. The MC@NLO generator uses the CTEQ6M1 set of parton distribution functions (PDFs), and all other simulated samples are generated using the CTEQ6L1 PDFs [57]. The $Z/\gamma^{\star}$ samples are normalized to the next-to-next-to-leading-order cross section computed with the FEWZ program [58]. We separately simulate $Z/\gamma^{\star}$ accompanied by heavy-flavor quarks ($b\bar{b}$ or $c\bar{c}$) using ALPGEN, and enhance the corresponding LO cross sections by a factor estimated from the NLO values computed with the MCFM program [59]. The diboson samples are normalized to the NLO cross section calculated with MCFM.

In addition, we apply a correction to the $Z/\gamma^{\star}$ + jets simulation, based on data [60], to address a small discrepancy in the modeling of Z boson transverse momentum p_T^Z in the simulation.

In Z boson events the asymmetries defined in Eqs. (1) and (2) are not well modeled in the simulation, especially in the $e\mu$ channel for $Z/\gamma^{\star} \to \tau\tau \to e\nu\mu\nu$ events. We therefore apply an additional correction using PYTHIA 8 [61], which correctly takes into account the tau lepton polarization and spin correlations for the tau decays. This reweighting is explained in detail in Sec. V.

An interesting class of BSM models that can generate a large $t\bar{t}$ forward-backward asymmetry at tree level arises from the presence of a color-octet vector particle G_{μ}^a (the so-called axigluon) with large mass m_G and chiral couplings. To check the sensitivity of our measurements to such new phenomena, we generate two axigluon samples

TABLE I.　Asymmetries predicted by MC@NLO and by the two models of axigluons described in the text. Uncertainties reflect only the statistical MC contributions. All values are given in %.

	Model 1	Model 2	MC@NLO
$A^{\ell\ell}$	21.3 ± 0.6	11.3 ± 0.5	3.3 ± 0.1
A_{FB}^{ℓ}	14.9 ± 1.0	8.9 ± 0.8	2.4 ± 0.1

[62] and pass these events through the full D0 simulation and reconstruction programs. Model 1 has a right-handed coupling to the SM quarks of $0.8g_s$ (where $g_s = \sqrt{\alpha_s/4\pi}$ is the QCD coupling) and no left-handed coupling. The axigluon mass is set to 0.2 TeV and the width to 50 GeV. Model 2 has a right-handed coupling to light SM quarks of $-1.5g_s$, a coupling of $6g_s$ to the top quark, and no left-handed coupling, with the axigluon mass and width set to 2 TeV and 670 GeV, respectively. Table I summarizes the values of the asymmetry predicted by these two models. These models are in agreement with experimental constraints ($t\bar{t}$ resonance searches and dijet production) from the Tevatron and the LHC, but in slight tension with the $t\bar{t}$ production cross section measurements.

III. EVENT SELECTION AND ESTIMATION OF INSTRUMENTAL BACKGROUND

We follow the approach developed in Ref. [63] for the event selection, i.e. using the criteria listed below:

(i) For the *ee* and $\mu\mu$ channels, we select events that pass at least one single-lepton trigger, while for the $e\mu$ channel, we consider events selected through a mixture of single and multilepton triggers and lepton + jet triggers. Efficiencies for single electron and muon triggers are measured using $Z/\gamma^{\star} \to ee$ or $Z/\gamma^{\star} \to \mu\mu$ data, and found to be $\approx 99\%$ and $\approx 80\%$, respectively, for dilepton signal events. For the $e\mu$ channel, the trigger efficiency is $\approx 100\%$.

(ii) We require at least one $p\bar{p}$ interaction vertex in the interaction region with $|z| < 60$ cm, where z is the coordinate along the beam axis, and $z = 0$ is the center of the detector. At least three tracks with $p_T > 0.5$ GeV must be associated with this vertex.

(iii) We require at least two isolated leptons with $p_T > 15$ GeV, both originating from the same interaction vertex. We consider only muons within $|\eta_{\mathrm{det}}| < 2.0$ and electrons within $|\eta_{\mathrm{det}}| < 1.1$ or $1.5 < |\eta_{\mathrm{det}}| < 2.5$. The two highest-$p_T$ leptons in an event must have opposite electric charges.

(iv) To reduce the background from bremsstrahlung in the $e\mu$ final state, we require the distance in (η, ϕ) space between the electron and the muon trajectories to be $\mathcal{R}(e, \mu) > 0.3$.

(v) In the *ee* and $\mu\mu$ channels, we require at least two jets with $p_T > 20$ GeV. For the $e\mu$ channel, we consider two types of events: (i) events with at least

two jets ($e\mu$ 2 jets) and (ii) events that contain just one detected jet ($e\mu$ 1 jet).

(vi) The $t\bar{t}$ final state contains two b-quark jets. To improve separation between signal and background, we apply a selection on the value of the MVA discriminant that assigns the b-quark hypothesis to the two jets of largest p_T. We use different cutoffs of the MVA discriminant variable, corresponding to b-jet efficiencies of 84% in $e\mu$ 2 jets, 80% in ee, 78% in $\mu\mu$, and 60% in $e\mu$ 1-jet events, with background misidentification efficiencies, respectively, of 23%, 12%, 7%, and 4%.

(vii) To improve signal purity, additional selection criteria are implemented based on global event properties of the final state. In the $e\mu$ 1-jet events, we require $H_T > 85$ GeV, where H_T is the scalar sum of the transverse momenta of the leading lepton and the leading jet. In the $e\mu$ 2-jets events, we require $H_T > 108$ GeV, where H_T is the scalar sum of the transverse momenta of the leading lepton and the two leading jets. In the ee final state, we require $\mathcal{S}(\not{E}_T) > 5$, while in the $\mu\mu$ channel, we require $\not{E}_T > 40$ GeV and $\mathcal{S}(\not{E}_T) > 2.5$.

(viii) All leptons must have $|\eta| < 2$ and a difference in rapidity of $|\Delta\eta| < 2.4$. These criteria reduce the statistical uncertainty on the calculated parton-level asymmetries (see Sec. IV).

The cutoff values of the selection criteria in items (vi) and (vii) are determined by minimizing the statistical uncertainty on the background-subtracted asymmetries (defined in Sec. IV).

To estimate the $t\bar{t}$ signal efficiency and the background contamination, we use MC simulation for all contributions except for the instrumental background, which is estimated from data.

In the ee and $e\mu$ channels, we determine the contributions from events with jets misidentified as electrons using the "matrix method" [64]. The loose sample of events (n_{loose}) is defined following the same selection as used for the $t\bar{t}$ candidate sample in items (i)–(vii) above, but ignoring the requirement on the electron MVA discriminant. For the dielectron channel, we drop the MVA requirement on one of the electrons chosen randomly.

We measure the efficiency ε_e that events with a true electron pass the requirement on the electron MVA

discriminant using $Z/\gamma^\star \rightarrow ee$ data. We measure the efficiency f_e that events with a misidentified jet pass the electron MVA requirement using $e\mu$ events chosen with selection criteria items (i)–(v), but requiring leptons of the same electric charge. For muons, we also apply a reversed isolation requirement: $E_T^{\mu,\text{iso}}/p_T^\mu > 0.2$, $p_T^{\mu,\text{iso}}/p_T^\mu > 0.2$, and $\not{E}_T < 15$ GeV, to minimize the contribution from $W + $ jets events.

We extract the number of events with jets misidentified as electrons (n_f), and the number of events with true electrons (n_e), by solving the equations:

$$n_{\text{loose}} = n_e/\varepsilon_e + n_f/f_e, \qquad (3)$$

$$n_{\text{tight}} = n_e + n_f, \qquad (4)$$

where n_{tight} is the number of events remaining after implementing the selections (i)–(vii). The factors f_e and ε_e are measured separately for each jet multiplicity (0, 1, and 2 jets), and separately for electron candidates in the CC and EC parts of the calorimeter. Typical values of ε_e are 0.7–0.8 in the CC and 0.65–0.75 in the EC. Values of f_e are 0.005–0.010 in the CC, and 0.005–0.020 in the EC.

In the $e\mu$ and $\mu\mu$ channels, we determine the number of events with an isolated muon arising from decays of hadrons in jets relying on the same selection as for the $e\mu$ or $\mu\mu$ channels, but requiring that both leptons have the same charge. In the $\mu\mu$ channel, this number of events is taken to be the number of same-sign events. In the $e\mu$ channel, it is the number of events in the same-sign sample after subtracting the contribution from events with jets misidentified as electrons.

The numbers of predicted background events, as well as the expected numbers of signal events, in the four channels are given in Table II and show high signal purity of the selected sample.

To complete the asymmetry measurement, we must determine not only the total number of events arising from instrumental background, but also their distributions in $q \times \eta$ and $\Delta\eta$. To determine these distributions for this background in the ee and $e\mu$ channels, we use the loose selection described above and implement a veto on events with one tight electron ($e\mu$ channel) or two tight electrons (ee channel). The residual contributions of the Z boson and diboson processes, as well as the expected contribution

TABLE II. Numbers of total expected (N_{expected}) and observed (N_{observed}) events from backgrounds and $t\bar{t}$ signal assuming the SM cross section (7.45 pb for a top quark mass of $m_t = 172.5$ GeV [65]). Expected numbers of events are shown with their statistical uncertainties. The uncertainty on the ratio of $N_{\text{observed}}/N_{\text{expected}}$ takes into account the statistical uncertainty on N_{observed} and N_{expected}.

	$Z \rightarrow \ell\ell$	Dibosons	Multijet and $W + $ jets	$t\bar{t} \rightarrow \ell\ell jj$	N_{expected}	N_{observed}	$\frac{N_{\text{observed}}}{N_{\text{expected}}}$
ee	$17.2^{+0.6}_{-0.6}$	$2.4^{+0.1}_{-0.1}$	$4.7^{+0.4}_{-0.4}$	$127.8^{+1.4}_{-1.4}$	$152.1^{+1.6}_{-1.6}$	147	0.97 ± 0.08
$e\mu$ 2 jets	$13.7^{+0.5}_{-0.5}$	$3.9^{+0.2}_{-0.2}$	$16.3^{+4.0}_{-4.0}$	$314.7^{+1.1}_{-1.1}$	$348.6^{+4.2}_{-4.2}$	343	0.98 ± 0.05
$e\mu$ 1 jet	$8.7^{+0.6}_{-0.6}$	$3.4^{+0.2}_{-0.2}$	$2.9^{+1.7}_{-1.7}$	$61.7^{+0.5}_{-0.5}$	$76.7^{+1.9}_{-1.9}$	78	1.02 ± 0.12
$\mu\mu$	$17.5^{+0.6}_{-0.6}$	$1.9^{+0.1}_{-0.1}$	$0.0^{+0.0}_{-0.0}$	$97.7^{+0.6}_{-0.6}$	$117.1^{+0.8}_{-0.8}$	114	0.97 ± 0.09

from the $t\bar{t}$ events, are subtracted. In the $\mu\mu$ channel, we use the same-sign events, where each of the muons is taken to have alternatively a negative and positive charge. The resulting distributions are normalized to the number of previously estimated background events.

IV. METHOD

Figure 1 presents the $q \times \eta$ and $\Delta\eta$ distributions for dilepton events after applying all but item (viii) of the selection criteria. We compute A_{FB}^{ℓ} and $A^{\ell\ell}$ in two steps. First, within each of the four channels, we perform a bin-by-bin subtraction of the estimated background contributions to the data. The lepton pseudorapidities are measured in D0 with a resolution better than 1% resulting in negligible migration effects. We therefore apply a simple bin-by-bin correction, which suffices to account

for the efficiency of reconstruction and selection requirements. The correction function is determined using $t\bar{t}$ MC@NLO events at the parton level within the fiducial region $|\eta| < 2$, $|\Delta\eta| < 2.4$ (here η refers to the generated lepton pseudorapidity) and events after reconstruction and selection. The asymmetries in the $q \times \eta$ and $\Delta\eta$ distributions after correction for selection efficiency are referred as "corrected" asymmetries. Figure 2 shows the corrected distributions for data compared to the predictions from MC@NLO. The cross section in each bin is calculated as a weighted sum of the measurements in all channels, where only the statistical uncertainty is taken into account.

In the second step, we extrapolate the corrected asymmetries to the full range of η by multiplying the corrected asymmetries with the calculated extrapolation factor,
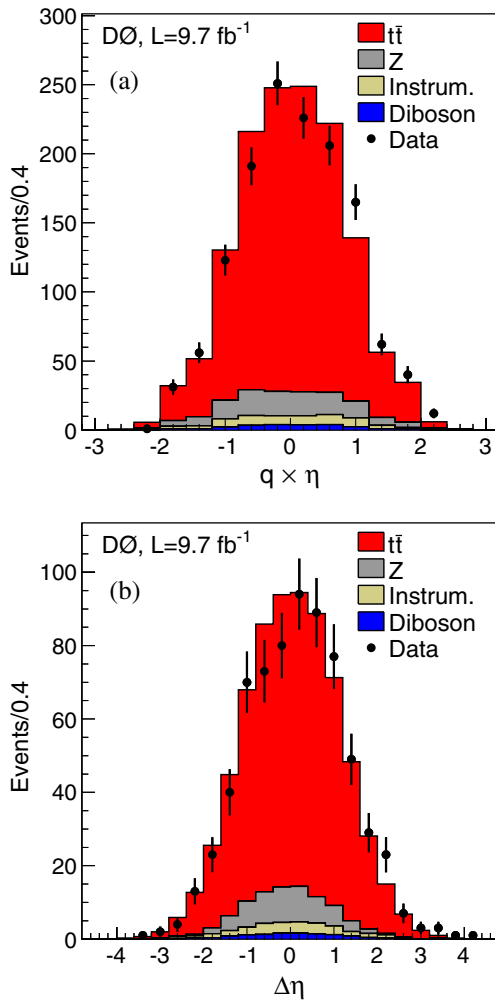

FIG. 1 (color online). Distributions in (a) $q \times \eta$ and (b) $\Delta\eta = \eta_{\ell^+} - \eta_{\ell^-}$, for the sum of ee, $e\mu$ and $\mu\mu$ channels, along with predictions of the backgrounds and $t\bar{t}$ signal. The black points show data events and the error bars indicate the statistical uncertainty on the data. Predicted events in the distributions are ordered in the same way as in the legend.
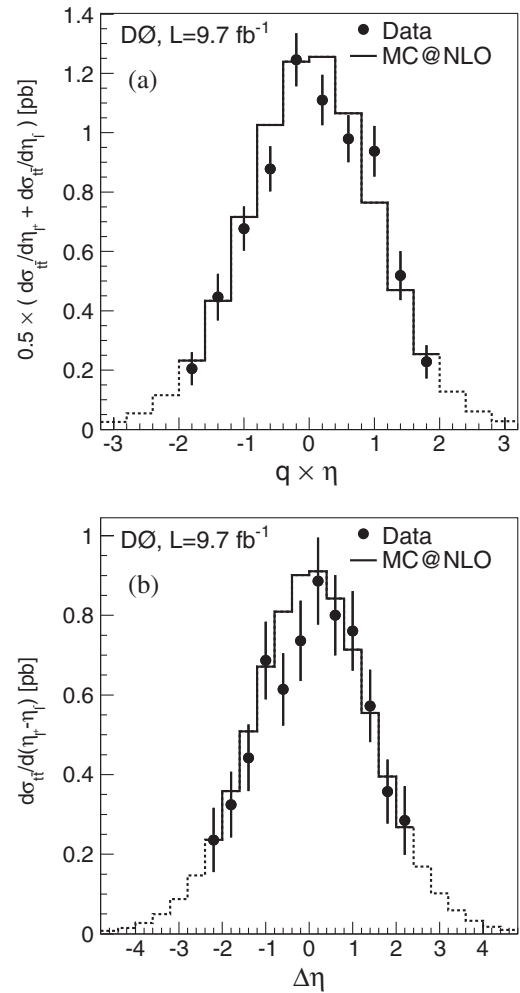
FIG. 2. Distributions in (a) $q \times \eta$ and (b) $\Delta\eta$, for the combined ee, $e\mu$, and $\mu\mu$ channels after subtraction of background and correction for selection efficiency within the acceptance. The error bars indicate the statistical uncertainty on data. The dashed lines show the predictions from MC@NLO outside the analysis acceptance.

which is given by the ratio of the generator level SM $t\bar{t}$ asymmetries from MC@NLO without selections to asymmetries within the fiducial region ($|\eta| < 2$ and $|\Delta\eta| < 2.4$). We refer to these asymmetries as "extrapolated" asymmetries. The exact values of the $|\eta|$ and $|\Delta\eta|$ requirements are chosen to optimize the expected statistical precision of the extrapolated asymmetries.

V. SYSTEMATIC UNCERTAINTIES

Systematic effects can affect the measured asymmetries in different ways: (i) they can change the normalization or the differential dependence, i.e., "shape," of the background distributions, (ii) they can affect the efficiency corrections and thereby modify the corrected and extrapolated asymmetries, and (iii) different MC generators or model assumptions can impact the extrapolation to all phase space. For item (iii), we verify that when axigluon MC samples (see Sec. II and Table I for predicted asymmetries) are used instead of MC@NLO to compute the extrapolation factor, we get consistent extrapolation factors. This shows that the model assumed for the extrapolation does not significantly affect the extrapolated correction.

We first consider the following sources of the systematic uncertainty: uncertainties on the efficiencies of electron and muon identification, uncertainties on trigger efficiencies, and uncertainties on jet-related quantities. The latter include contributions from the uncertainty in jet energy scale, jet energy resolution, jet identification efficiency, and b-quark jet tagging efficiency. All of these systematic uncertainties are propagated to the background distributions and to the corrections for $t\bar{t}$ signal efficiency; they are found to be small and are grouped into the object identification (Object ID) category.

Next, we consider uncertainties specific to the background model. These include uncertainties on the asymmetries generated for Z boson events (see Sec. II) and on background normalization, which is typically $\approx 10\%$. The background normalization uncertainty accounts for the uncertainties on the integrated luminosity [66], object ID efficiency, b-tagging identification efficiency, and theoretical background cross sections. We also calibrate our ability to reconstruct angular asymmetries by comparing asymmetries observed for Z bosons in data with MC simulation. We use samples with requirements (i)–(iv) only and ignore any jet selection in order to have a significant number of events and therefore a small statistical uncertainty on the asymmetry ($\approx 0.13\%$ in data and $\approx 0.04\%$ in simulation). We verify that we can reproduce the asymmetries observed in data if we reweight the MC distributions using distributions obtained with PYTHIA 8 [61]. This reweighting is based on the ratio of two-dimensional distributions in (η_{ℓ^+}, η_{ℓ^-}) space for ALPGEN and PYTHIA 8. After requiring one or two jets, we observe a residual difference between the data and MC asymmetries in a

TABLE III. Systematic uncertainties for the corrected and the extrapolated asymmetries. All values are given in %.

Source	Corrected		Extrapolated	
	A_{FB}^{ℓ}	$A^{\ell\ell}$	A_{FB}^{ℓ}	$A^{\ell\ell}$
Object ID	0.54	0.50	0.59	0.60
Background	0.66	0.74	0.72	0.88
Hadronization	0.52	0.62	0.62	0.92
MC statistics	0.19	0.23	0.23	0.37
Total	1.02	1.12	1.14	1.46

sample dominated by background obtained by reversing the b-quark-tagging requirement (vi). We take this difference as a systematic uncertainty on the contribution from the Z boson background.

The most significant contribution to the background-related uncertainty is from the uncertainty on instrumental background. We estimate this by changing the amount of instrumental background according to the uncertainty on its normalization. We also account for possible uncertainties in the distribution of instrumental background by changing the number of events in each bin of the instrumental background distribution by ± 1 SD of its statistical uncertainty. The changes are applied in opposite directions for the positive $q \times \eta \geq 0$ or $\Delta\eta \geq 0$ and negative $q \times \eta < 0$ or $\Delta\eta < 0$ parts of the distributions in order to maximize the effect.

Another important uncertainty is related to the choice of parton showering and hadronization in $t\bar{t}$ events. This is evaluated by taking the difference between the asymmetries obtained with efficiency corrections and extrapolation factors using MC@NLO + HERWIG and ALPGEN + PYTHIA. This estimation also includes the difference in the simulation of NLO effects between MC@NLO and ALPGEN generators.

Finally, we consider the limited statistics of the MC samples used to measure the efficiency correction. These provide the smallest contributions to the systematic uncertainties on the extracted asymmetries. All the above systematic uncertainties are listed in Table III.

As shown in the following section, the main uncertainty on the measured asymmetries is due to the limited size of the data sample.

VI. RESULTS

We combine the asymmetries measured in the ee, $e\mu$ 2-jets, $e\mu$ 1-jet, and $\mu\mu$ channels using the BLUE method [67,68], assuming 100% correlation among their systematic uncertainties. Table IV summarizes the corrected and extrapolated asymmetries, as well as the prediction from a SM NLO calculation including QCD and electroweak (EW) corrections [41]. The measured values are consistent with theoretical predictions based on the SM.

TABLE IV. The measured corrected and extrapolated asymmetries defined in Eqs. (1) and (2) for all channels separately and combined, compared to the predicted SM NLO asymmetries [41] for inclusive $t\bar{t}$ production. The measured extrapolated asymmetry should be compared with the SM NLO prediction. The first uncertainty on the measured values corresponds to the statistical and the second to the systematic contribution. All values are given in %. The uncertainty on the SM NLO predictions is due to renormalization and factorization scale variations.

	Corrected	Extrapolated	Prediction
A_{FB}^{ℓ}			
ee	$6.8 \pm 8.5 \pm 1.3$		
$e\mu$ 2 jets	$5.0 \pm 4.6 \pm 1.0$		
$e\mu$ 1 jet	$-0.1 \pm 10.4 \pm 2.5$		
$\mu\mu$	$0.8 \pm 8.5 \pm 1.4$		
Combined	$4.1 \pm 3.5 \pm 1.0$	$4.4 \pm 3.7 \pm 1.1$	3.8 ± 0.3
$A^{\ell\ell}$			
ee	$16.4 \pm 10.4 \pm 1.6$		
$e\mu$ 2 jets	$11.1 \pm 6.3 \pm 1.3$		
$e\mu$ 1 jet	$-2.1 \pm 15.7 \pm 3.4$		
$\mu\mu$	$7.4 \pm 11.7 \pm 1.4$		
Combined	$10.5 \pm 4.7 \pm 1.1$	$12.3 \pm 5.4 \pm 1.5$	4.8 ± 0.4

In addition, we study the dependence of the corrected asymmetries as a function of $q \times \eta$ and $\Delta\eta$ in Fig. 3, where we observe no significant dependence on these variables in the data and consistency with the MC@NLO [51,52] predictions. Figure 3 also shows the comparison with the two axigluon models described in Sec. II.

To study the statistical correlation between A_{FB}^{ℓ} and $A^{\ell\ell}$, we assume that positive and negative leptons have identical rapidity distributions, and we use the lepton $q \times \eta$ distribution in data (Fig. 2) as the basis for generating an ensemble of $q \times \eta$ distributions. The residual reconstruction level differences between positive and negative lepton distributions are made negligible by the regular flip of the solenoid and toroid polarities during the data taking. The number of events in each bin is drawn from a Gaussian distribution with mean equal to the number of events in the bin of the initial distribution and width equal to the statistical uncertainty on the number of events. The resulting distributions are used as probability density functions to generate pairs of rapidity values for positive and negative leptons (η_{l^+}, η_{l^-}). Since the value of η for each lepton is generated independently, there is no direct correlation between them. Repeating this procedure many times, we form the $\Delta\eta = \eta_{\ell^+} - \eta_{\ell^-}$ distribution and calculate both the A_{FB}^{ℓ} and $A^{\ell\ell}$ asymmetries. Using the (A_{FB}^{ℓ}, $A^{\ell\ell}$) pairs generated in this way, we measure the correlation between the two asymmetries to be 0.82. We verify that the value of $A^{\ell\ell}$ obtained with the same method but using the MC $q \times \eta$ event distribution as input accurately reproduces the simulated asymmetry from MC@NLO and axigluon models. Using this correlation coefficient, we can compute
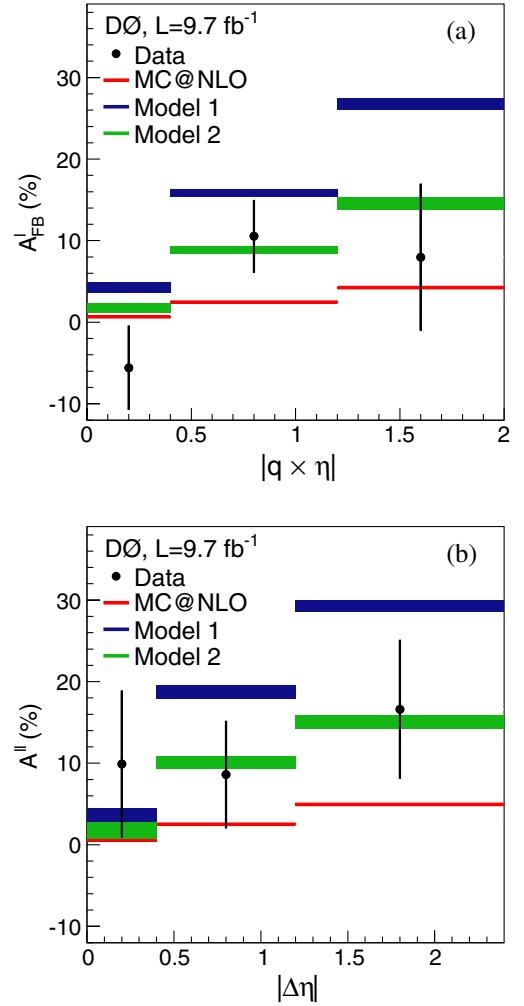

FIG. 3 (color online). Asymmetry distributions in (a) $|q \times \eta|$ and (b) $|\Delta\eta| = |\eta_{\ell^+} - \eta_{\ell^-}|$, for the combined ee, $e\mu$, and $\mu\mu$ channels after background subtraction and after corrections for selection efficiency. The error bars indicate statistical uncertainties on the data. The data are compared with expectations from MC@NLO and axigluon Model 1 and Model 2 as defined in the text.

the ratio of the two extrapolated asymmetries in data to be $R = A_{\mathrm{FB}}^{\ell}/A^{\ell\ell} = 0.36 \pm 0.20$, consistent at the level of 2 SDs with the prediction of 0.79 ± 0.10. The uncertainty on the theoretical ratio is estimated by adding in quadrature the uncertainty on the theoretical expectations for A_{FB}^{ℓ} and $A^{\ell\ell}$ and without taking into account the possible correlation between these two values. This predicted ratio is found to be almost the same for the different tested models as can be seen in Fig. 4.

The mean value of $A^{\ell\ell}$ measured in this analysis differs from that in our previous measurement [38], but is compatible. The change in central value is due to changes in object identification and event selections (in particular, the use of b-quark jet identification) that improve the signal-to-background ratio and significantly reduce all systematic uncertainties related to background contributions, which affects the central values of the results.
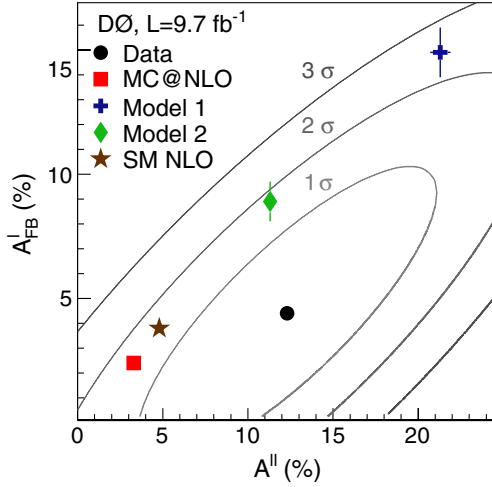
FIG. 4 (color online). Extrapolated A_{FB}^ℓ versus $A^{\ell\ell}$ asymmetries in $t\bar{t}$ data, the predictions from MC@NLO, axigluon models, and from the latest SM NLO prediction [41]. The ellipses represent contours of total uncertainty at 1, 2, and 3 SDs on the measured result. All values are given in %. Predicted asymmetries are shown with their statistical uncertainties.

VII. CONCLUSION

We have presented measurements of asymmetries in angular distributions of leptons produced in $t\bar{t}$ dilepton final states. Using the full Run II Tevatron data set recorded by the D0 detector, we measure the single lepton and dilepton asymmetries, corrected for reconstruction efficiency as

$$A_{FB}^\ell = (4.1 \pm 3.5(\text{stat}) \pm 1.0(\text{syst}))\%,$$
$$|\eta| < 2.0, \qquad |\Delta\eta| < 2.4,$$

and

$$A^{\ell\ell} = (10.5 \pm 4.7(\text{stat}) \pm 1.1(\text{syst}))\%,$$
$$|\eta| < 2.0, \qquad |\Delta\eta| < 2.4.$$

In addition, extrapolating these asymmetries for acceptance selections yields the inclusive $t\bar{t}$ lepton asymmetries:

$$A_{FB}^\ell = (4.4 \pm 3.7(\text{stat}) \pm 1.1(\text{syst}))\%,$$

and

$$A^{\ell\ell} = (12.3 \pm 5.4(\text{stat}) \pm 1.5(\text{syst}))\%.$$

These values are compatible with the SM NLO calculation that includes QCD and EW corrections [41]. We have studied the correlation between A_{FB}^ℓ and $A^{\ell\ell}$ and computed the ratio of the two asymmetries, which also shows agreement with calculations based on the standard model.

APPENDIX: DIFFERENTIAL ASYMMETRY TABLES

Table V shows the $t\bar{t}$ differential cross section in bins of $q \times \eta$ and $\Delta\eta$ as shown in Fig. 2. $\frac{1}{2} \times (\frac{d\sigma_{t\bar{t}}}{d\eta_{l^+}} + \frac{d\sigma_{t\bar{t}}}{d\eta_{l^-}})$ represents the $t\bar{t}$ differential cross section in $q \times \eta$ and $\frac{d\sigma_{t\bar{t}}}{d(\eta_{l^+} - \eta_{l^-})}$ the $t\bar{t}$ differential cross section in $\Delta\eta$. Table VI shows the values of the asymmetries in different angular regions as shown in Fig. 3.

TABLE V. $t\bar{t}$ cross section in each bin of Fig. 2.

Bin	$\frac{1}{2} \times (\frac{d\sigma_{t\bar{t}}}{d\eta_{l^+}} + \frac{d\sigma_{t\bar{t}}}{d\eta_{l^-}})$ [pb]	$\frac{d\sigma_{t\bar{t}}}{d(\eta_{l^+} - \eta_{l^-})}$ [pb]
$-2.4, -2.0$	0.0	0.236 ± 0.081
$-2.0, -1.6$	0.205 ± 0.056	0.325 ± 0.082
$-1.6, -1.2$	0.446 ± 0.078	0.442 ± 0.084
$-1.2, -0.8$	0.677 ± 0.075	0.686 ± 0.097
$-0.8, -0.4$	0.878 ± 0.076	0.614 ± 0.091
$-0.4, 0.0$	1.245 ± 0.089	0.736 ± 0.101
$0.0, 0.4$	1.110 ± 0.085	0.886 ± 0.109
$0.4, 0.8$	0.979 ± 0.079	0.800 ± 0.101
$0.8, 1.2$	0.937 ± 0.085	0.761 ± 0.100
$1.2, 1.6$	0.518 ± 0.082	0.572 ± 0.091
$1.6, 2.0$	0.228 ± 0.056	0.357 ± 0.081
$2.0, 2.4$	0.0	0.285 ± 0.086

TABLE VI. Value of the asymmetries in different bins of the distributions of Fig. 3.

$|q \times \eta|$ bin	A_{FB}^ℓ
0.0, 0.4	-0.061 ± 0.052
0.4, 1.2	0.103 ± 0.045
1.2, 2.0	0.057 ± 0.101

$|\Delta\eta|$ bin	$A^{\ell\ell}$
0.0, 0.4	0.092 ± 0.091
0.4, 1.2	0.083 ± 0.066
1.2, 2.4	0.125 ± 0.088

[1] F. Abe *et al.* (CDF Collaboration), Phys. Rev. Lett. **74,** 2626 (1995).

[2] S. Abachi *et al.* (D0 Collaboration), Phys. Rev. Lett. **74,** 2632 (1995).

[3] W. Bernreuther and Z.-G. Si, Nucl. Phys. B **837,** 90 (2010).

[4] W. Hollik and D. Pagani, Phys. Rev. D **84,** 093003 (2011).

[5] V. Ahrens, A. Ferroglia, M. Neubert, B. D. Pecjak, and L. L. Yang, Phys. Rev. D **84,** 074004 (2011).

[6] J. H. Kuhn and G. Rodrigo, J. High Energy Phys. 01 (2012) 063.

[7] P. Ferrario and G. Rodrigo, Phys. Rev. D **78,** 094018 (2008).

[8] P. Ferrario and G. Rodrigo, Phys. Rev. D **80,** 051701 (2009).

[9] O. Antunano, J. H. Kuhn, and G. Rodrigo, Phys. Rev. D **77,** 014003 (2008).

[10] P. H. Frampton, J. Shu, and K. Wang, Phys. Lett. B **683,** 294 (2010).

[11] D.-W. Jung, P. Ko, J. S. Lee, and S.-H. Nam, Phys. Lett. B **691,** 238 (2010).

[12] A. Arhrib, R. Benbrik, and C.-H. Chen, Phys. Rev. D **82,** 034034 (2010).

[13] A. Djouadi, G. Moreau, F. Richard, and R. K. Singh, Phys. Rev. D **82,** 071702 (2010).

[14] E. Alvarez, L. Da Rold, J. I. S. Vietto, and A. Szynkman, J. High Energy Phys. 09 (2011) 007.

[15] C.-H. Chen, G. Cvetic, and C. Kim, Phys. Lett. B **694,** 393 (2011).

[16] D.-W. Jung, P. Ko, and J. S. Lee, Phys. Lett. B **701,** 248 (2011).

[17] J. Aguilar-Saavedra and M. Perez-Victoria, Phys. Lett. B **705,** 228 (2011).

[18] G. Marques Tavares and M. Schmaltz, Phys. Rev. D **84,** 054008 (2011).

[19] R. Barcelo, A. Carmona, M. Masip, and J. Santiago, Phys. Lett. B **707,** 88 (2012).

[20] K. Cheung, W.-Y. Keung, and T.-C. Yuan, Phys. Lett. B **682,** 287 (2009).

[21] B. Xiao, Y.-k. Wang, and S.-h. Zhu, Phys. Rev. D **82,** 034026 (2010).

[22] Q.-H. Cao, D. McKeen, J. L. Rosner, G. Shaughnessy, and C. E. Wagner, Phys. Rev. D **81,** 114004 (2010).

[23] S. Jung, H. Murayama, A. Pierce, and J. D. Wells, Phys. Rev. D **81,** 015004 (2010).

[24] J. Cao, Z. Heng, L. Wu, and J. M. Yang, Phys. Rev. D **81,** 014016 (2010).

[25] V. Barger, W.-Y. Keung, and C.-T. Yu, Phys. Rev. D **81,** 113009 (2010).

[26] P. Ko, Y. Omura, and C. Yu, Phys. Rev. D **85,** 115010 (2012).

[27] P. Ko, Y. Omura, and C. Yu, J. High Energy Phys. 01 (2012) 147.

[28] P. Ko, Y. Omura, and C. Yu, Eur. Phys. J. C **73,** 2269 (2013).

[29] M. Bauer, F. Goertz, U. Haisch, T. Pfoh, and S. Westhoff, J. High Energy Phys. 11 (2010) 039.

[30] R. S. Chivukula, E. H. Simmons, and C.-P. Yuan, Phys. Rev. D **82,** 094009 (2010).

[31] I. Dorsner, S. Fajfer, J. F. Kamenik, and N. Kosnik, Phys. Rev. D **81,** 055009 (2010).

[32] J. Shu, T. M. Tait, and K. Wang, Phys. Rev. D **81,** 034012 (2010).

[33] J. Aguilar-Saavedra and M. Perez-Victoria, J. High Energy Phys. 09 (2011) 097.

[34] T. Aaltonen *et al.* (CDF Collaboration), Phys. Rev. D **87,** 092002 (2013).

[35] V. M. Abazov *et al.* (D0 Collaboration), Phys. Rev. D **84,** 112005 (2011).

[36] The pseudorapidity η is defined as a function of the polar angle θ with respect to the proton beam as $\eta = -\ln(\tan\frac{\theta}{2})$. Positive (negative) η corresponds to a particle produced in the direction of the incoming proton (antiproton).

[37] T. Aaltonen *et al.* (CDF Collaboration), arXiv:1308.1120.

[38] V. M. Abazov *et al.* (D0 Collaboration), Phys. Rev. D **87,** 011103(R) (2013).

[39] G. Aad *et al.* (ATLAS Collaboration), Eur. Phys. J. C **72,** 2039 (2012).

[40] S. Chatrchyan *et al.* (CMS Collaboration), Phys. Lett. B **717,** 129 (2012).

[41] W. Bernreuther and Z.-G. Si, Phys. Rev. D **86,** 034026 (2012).

[42] V. M. Abazov *et al.* (D0 Collaboration), Nucl. Instrum. Methods Phys. Res., Sect. A **565,** 463 (2006).

[43] R. Angstadt *et al.* (D0 Collaboration), Nucl. Instrum. Methods Phys. Res., Sect. A **622,** 298 (2010).

[44] M. Abolins *et al.*, Nucl. Instrum. Methods Phys. Res., Sect. A **584,** 75 (2008).

[45] S. Abachi *et al.* (D0 Collaboration), Nucl. Instrum. Methods Phys. Res., Sect. A **338,** 185 (1994).

[46] V. M. Abazov *et al.* (D0 Collaboration), Nucl. Instrum. Methods Phys. Res., Sect. A **552,** 372 (2005).

[47] V. M. Abazov *et al.* (D0 Collaboration), arXiv:1307.5202.

[48] G. C. Blazey *et al.*, arXiv:hep-ex/0005012.

[49] V. M. Abazov *et al.* (D0 Collaboration), Nucl. Instrum. Methods Phys. Res., Sect. A **620,** 490 (2010).

[50] R. Brun and F. Carminati, CERN Program Library Long Writeup W5013, 1993 (unpublished).

[51] S. Frixione and B. R. Webber, J. High Energy Phys. 06 (2002) 029.

[52] S. Frixione and B. R. Webber, arXiv:0812.0770.

[53] G. Corcella, I. G. Knowles, G. Marchesini, S. Moretti, K. Odagiri, P. Richardson, M. H. Seymour, and B. R. Webber, J. High Energy Phys. 01 (2001) 010.

[54] M. L. Mangano, F. Piccinini, A. D. Polosa, M. Moretti, and R. Pittau, J. High Energy Phys. 07 (2003) 001.

[55] T. Sjostrand, S. Mrenna, and P. Z. Skands, J. High Energy Phys. 05 (2006) 026.

[56] T. Affolder *et al.* (CDF Collaboration), Phys. Rev. D **65,** 092002 (2002).

[57] P. M. Nadolsky, H.-L. Lai, Q.-H. Cao, J. Huston, J. Pumplin, D. Stump, W.-K. Tung, and C.-P. Yuan, Phys. Rev. D **78,** 013004 (2008).

[58] R. Gavin, Y. Li, F. Petriello, and S. Quackenbush, Comput. Phys. Commun. **182,** 2388 (2011).

[59] R. K. Ellis, Nucl. Phys. B, Proc. Suppl. **160,** 170 (2006).

[60] V. M. Abazov *et al.* (D0 Collaboration), Phys. Lett. B **693,** 522 (2010).

[61] T. Sjostrand, S. Mrenna, and P. Z. Skands, Comput. Phys. Commun. **178,** 852 (2008).

[62] A. Falkowski, M. L. Mangano, A. Martin, G. Perez, and J. Winter, Phys. Rev. D **87**, 034039 (2013).

[63] V. M. Abazov *et al.* (D0 Collaboration), Phys. Lett. B **704**, 403 (2011).

[64] V. Abazov *et al.* (D0 Collaboration), Phys. Rev. D **76**, 092007 (2007).

[65] S. Moch and P. Uwer, Phys. Rev. D **78**, 034003 (2008).

[66] T. Andeen *et al.* (D0 Collaboration), Report No. FERMILAB-TM-2365, 2007.

[67] A. Valassi, Nucl. Instrum. Methods Phys. Res., Sect. A **500**, 391 (2003).

[68] L. Lyons, D. Gibaut, and P. Clifford, Nucl. Instrum. Methods Phys. Res., Sect. A **270**, 110 (1988).